ZIBELINE INTERNATIONAL™ PUBLISHING

ISSN: 2521-0920 (Print)
ISSN: 2521-0602 (Online)
CODEN: MJGAAN

Malaysian Journal of Geosciences (MJG)

DOI: http://doi.org/10.26480/mjg.01.2023.22.30

RESEARCH ARTICLE

AEROMAGNETIC INVESTIGATION OF THE BANDED IRON FORMATIONS OF UM NAR AREA, CENTRAL EASTERN DESERT, EGYPT

Atef M. Abu Donia*

Studies department, Nuclear Materials Authority, P.O. Box (530) El-Maadi, Cairo, Egypt
Corresponding Author Email: atef_donia@yahoo.com

ARTICLE DETAILS

Article History:

Received 15 January 2022
Revised 01 February 2022
Accepted 02 March 2023
Available online 08 March 2023

ABSTRACT

Wadi Um Nar area acquired its importance since the discovery of banded iron formations (BIFs), and is one of the largest iron formation occurrences in the Eastern Desert of Egypt. Therefore, the recorded aeromagnetic data were processed, using a combination of edge enhancement filters, to identify major structures and recognize the lateral and vertical distribution of BIFs, as well as to determine the locations of buried magnetite ore bodies in this area. The obtained results from the application of these techniques revealed that the NW–SE, NE–SW and N–S directions are the common tectonic trends in the region. These trends could be faults or shear zones that have acted as good pathway or channels for hydrothermal fluids. Estimating the basement depth using source parameter imaging (SPI) showed that the BIFs depths varied from the surface down to about 450 m. Additionally, the orthogonal derivative maps of Wadi Um Nar BIFs showed an E–W trend, which corresponds exactly to the maximum magnetic intensity belt and their anomalies are characterized by a distinct dipole nature. These maps also revealed the extent and continuity of the main ore body of BIFs and showed that, they were mainly produced from magnetite mineral, formed in regions of structurally-controlled fluid flow.

Keywords

Wadi Um Nar; Aeromagnetic Data; Banded Iron Formations; Edge Enhancement Techniques; Structure.

1. INTRODUCTION

Magnetic survey is widely used in mineral prospecting for regional-scale resource mapping and for detailed characterization of mineral ore deposits at site-scale (Telford et al., 1990; Silva, 1999; Nabighian et al., 2005). Iron ore deposits are well-defined targets for magnetic methods, as ores rich in magnetite and hematite are easily identified by their high magnetic contrast to host rocks. The banded iron formations (BIFs) are economically essential because they are by far one the most important sources of iron ore deposits in the world (Bekker et al., 2010; Nadoll et al., 2014; Zhu et al., 2014; El Habaak, 2021). BIFs are widely recognized as chemical precipitation products for oxides and hydroxides of Fe^{2+} and Fe^{3+}, silicates rich in Fe, and silica as recorded in the marine environment. They are affected by prominent metamorphism and diagenetic processes (Klein and Beukes, 1993; Mücke et al., 1996).

Egyptian BIFs occur in 13 areas, in a space of thirty-thousand km^2, in the Central Eastern Desert (CED) of Egypt, as illustrated on Figure 1. These deposits are categorized, according to Sims and James, as Algoma–type, despite the fact that they take place intercalated with volcanosedimentary Neoproterozoic units of intermediate composition instead of the typical Archean/Paleoproterozoic fundamental volcanic rocks related with most Algoma–type BIFs (Sims and James, 1984; El-Shazly et al., 2019; Gross, 1996; Klein, 2005; Bekker et al., 2010; El-Shazly and Khalil, 2014; El Habaak, 2021). BIF ore deposits are widely distributed in the metamorphic rocks such as greenschist and amphibolite facies during collision stage of Pan-African Orogeny (Loizenbauer et al., 2001; Ali et al., 2009; El-Shazly and Khalil, 2014; El Habaak, 2021).

Some authors characterize the formation of the BIF Neoproterozoic units to specific tectonic and/or volcanic events, or to big igneous provinces/super plumes, rather than global climatic changes (Isley, 1995; Isley and Abbott, 1999; Eyles and Januszczak, 2004; Ohmoto et al., 2006; Basta et al., 2011; Freitas et al., 2011; Stern et al., 2013). Every time, the emergence of BIFs in a region has worthy implications on the paleoenvironment and tectonics, necessitating their study for a good tectonic explanation (Stern et al., 2013; El-Shazly et al., 2019). Airborne magnetic methods constitute one of the most widely used geophysical techniques for geological interpretations, playing an important role in identifying geological features including faults, shear zones, folds, intrusions, porphyries and other areas preferred for mineralization. These structures are important in the exploration and localization of mineralization zones (e.g., Silva, 1999; Holden et al., 2012; Shah et al., 2013; Abdelrahman and Essa, 2015; Henderson et al., 2015; Abo-Ezz and Essa, 2016; Farhi et al., 2016; Essa and Elhussein, 2017; Elhussein and Shokry, 2020; Shebl et al., 2021; Ekwok et al., 2022; Essa and Diab, 2022; Boufkri et al., 2023; Elhusseiny, 2023).

Wadi Um Nar iron ore deposit (Figure 1, # 11) is one of the largest BIFs in Pan-African rocks in the CED of Egypt (El-Ramly et al., 1963). Wadi Um Nar region is structurally complex, with evidence of several deformation phases, as well as, various igneous intrusions that are spatially related to the iron ore (e.g., Akaad et al., 1996; Makroum, 2003; Shalaby et al., 2005, 2006; Stern et al., 2013). Although, Um Nar BIFs were the focus of many authors, due to their economic potential as the most lucrative sources of iron, leading to several excellent studies, but it still needs many of geophysical studies (El-Ramly et al., 1963; El Aref et al., 1993a, 1993b; Akaad et al., 1996; El Habaak, 2004; Shalaby et al., 2005; El-Shazly and Khalil, 2014; El Habaak, 2021). Geophysical methods are able to detect and identify local subsurface features of the ore body that cannot be detected by drilling programs. Thus, a geophysical survey can improve exploration programs by maximizing ground coverage rate and reducing drilling

Quick Response Code	Access this article online	
	Website: www.myjgeosc.com	DOI: 10.26480/mjg.01.2023.22.30

Cite The Article: Atef M. Abu Donia (2023). Aeromagnetic investigation of the banded iron formations of Um Nar area, Central Eastern Desert, Egypt. *Malaysian Journal of Geosciences, 7(1): 22-30.*

requirements.

The goals of this study are to supply a clear structural framework model of Wadi Um Nar BIFs area (Figure 1, # 11), located in the CED of Egypt. The specific objectives of the present study include: (1) applying several edge enhancement techniques to the aeromagnetic data to define the edges of magnetic sources (contacts and/or faults), (2) identification the vertical and lateral distributions of the BIFs, and (3) attempting to better understanding of the mode of occurrence of the BIFs in Um Nar and their relationship to the general structural framework.

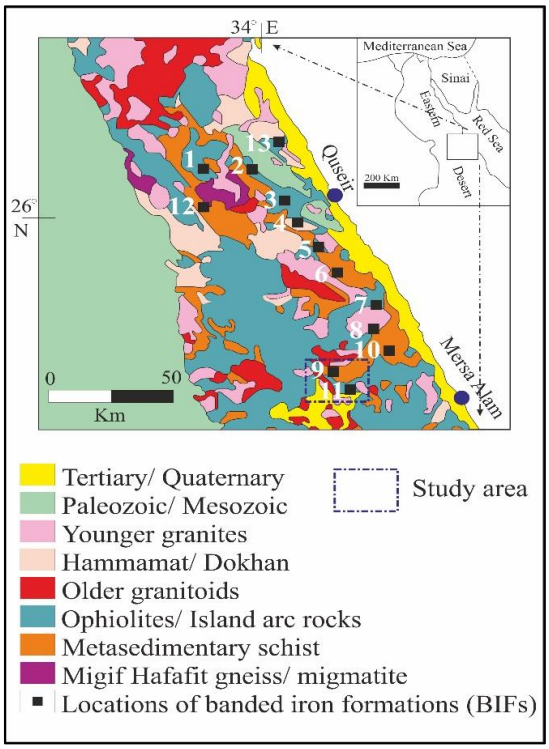

Figure 1: A simplified geologic map of the Central Eastern Desert of Egypt showing the locations of some banded iron formation (BIF) occurrences; 1 – Hadrabia; 2 – Abu Merwat; 3 – Gabal Semna; 4 – Diwan; 5 – Wadi Kareim; 6 – Wadi El Dabbah; 7 – Um Shaddad; 8 – Um Ghamis; 9 – Gabal El-Hadid; 10 – El Emra; 11 – Um Nar (study area); 12 – Wadi Hammama; 13 – Um Anab (Khalil et al., 2015).

2. Geological Setting

Several authors have described the geological settings of Wadi Mubarak-belt, which includes Wadi Um Nar (Figure 1, # 11; study area) region (Abu El Ela, 1985; Dardir and El Shimi, 1992; El Aref et al., 1993a, 1993b; El-Habaak and Mahmoud, 1994; Akaad et al., 1995, 1996; Makroum, 2003; Shalaby, 2003; Shalaby et al., 2005, 2006; Kassem, 2011, 2012; Stern et al., 2013; El-Shazly and Khalil, 2014; El Habaak, 2021). Wadi Mubarak could be described as discrete wedged shape of highly-deformed lower-grade greenschist rocks, bounded by metavolcanics (Akaad et al., 1996; Kassem, 2011, 2012). The deformed zone is well extended from the Red Sea coast in the eastern part to Gabal (G.) El-Hadid (bearing iron ore deposits) in the western part of the mapped area (Figure 1, # 9) (Akaad et al., 1996). The volcano-sedimentary sequence consists of metavolcanics and biotite schists, which are dissected by BIFs. This zone has an extension from G. El-Hadid northwest into Wadi Um Nar and G. El-Mayet southeast in the studied area (Figure 2), which shows varying topography changing from 423 m to 896 m above sea level (Figure 3). Rasmy (1968) separated the metasedimentary sequences into graphite–chlorite schist, hornblende biotite schist, biotite schist, pebbly quartz–biotite schist, in addition to actinolite–epidote schist.

The BIFs of Wadi Um Nar area are hosted in a metamorphosed clastic and calcareous sedimentary sequence, which represents the upper part of the ophiolitic mélange described by as shelf sedimentary rocks (El Aref et al., 1993a; 1993b; El Bahariya, 2018; 2021; El Habaak, 2021). The metamorphosed sedimentary succession has undergone several stages of brittle deformation. It constitutes a tight northwest–southeast striking and southwest dipping overturned anticline plunging very steeply to the southeast (El Habaak, 2004). There are two thrust faults bounding the metamorphosed rocks, as shown in Figure 2. The mylonitic gneiss rocks were intruded by granodiorite, post-tectonic granite, gabbro-olivine and felsite dikes. Granodiorite rock is represented by the G. El Umra in the northeastern part, meanwhile, the post-tectonic granite has small, scattered masses in the study area, presented in southwestern part (Figure 2). The post-tectonic granite is characterized by pink to reddish pink colour (El Habaak, 2004; 2021).

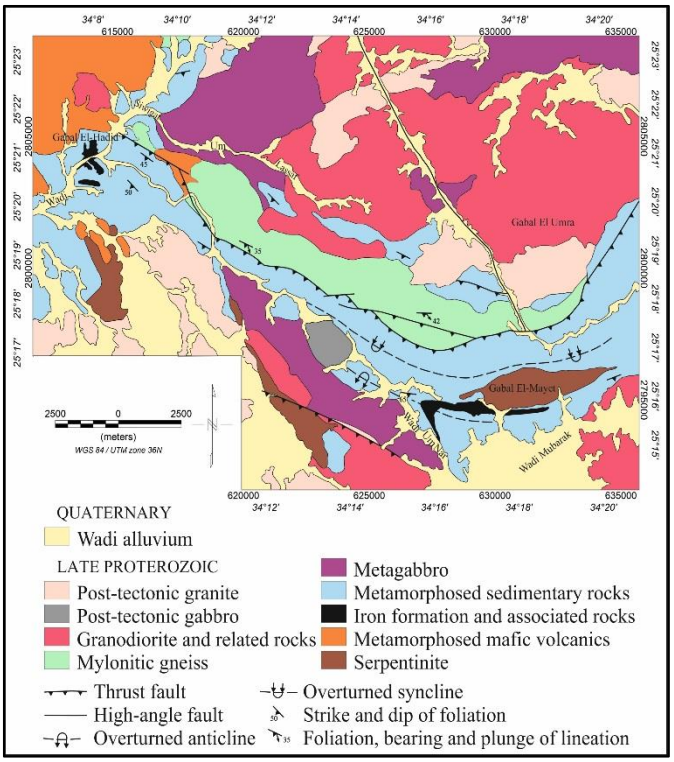

Figure 2: Geologic map of Wadi Um Nar area, Central Eastern Desert, Egypt (Sims and James, 1984; El Habaak, 2004).

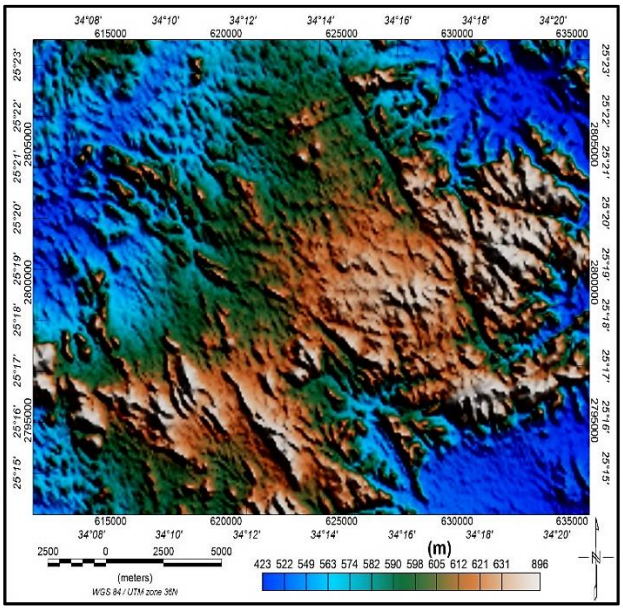

Figure 3: Shuttle Radar Topography Mission (SRTM) elevation map of Wadi Um Nar area, Central Eastern Desert, Egypt.

Granodiorite is medium grained, from equigranular to porphyritic in textures, and composed of plagioclase and amphibole phenocrysts reached up to 0.8 cm in diameter in addition to quartz. It is highly altered, whereas chlorite is the alteration product of amphiboles and biotite, and the sericite and kaolinite replace the plagioclase phenocrysts (El Habaak, 2004; 2021). BIFs are connected with biotite schist and consists of alternating Fe-rich and chert bands. Biotite schists are metamorphosed pelites and calc-silicate rocks. The intercalations of BIFs with clastic layers are good indicators for the deposition in low energy environment, as mentioned (El Habaak, 2004; 2021).

Wadi Um Nar was structurally affected by two different deformational events (Neumayr et al., 1998; Loizenbauer et al., 2001; Makroum, 2003;

Stern et al., 2013; El-Shazly and Khalil, 2014). The first stage identified as folding-thrusting episode resulted in a tight WNW–ESE striking and SW dipping overturned anticline plunging very steeply to the SE. BIFs have a lateral extension, running along strike of Wadi Um Nar anticline. A series of E–W striking and south-dipping thrusts also resulted due to the first deformational phase leading to emplacement of allochthonous sheets, where BIFs run in the E–W direction, parallel to the serpentinite mass of G. El-Mayet (El-Shazly and Khalil, 2014). The second deformational phase produced a synform with a NW–SE trend and southeast-plunging axis. It has been interpreted that the southwestern limb was thrusted onto the northeastern limb. In the southwestern limb, BIFs extend along the eastern side of Wadi Um Nar.

3. Data Acquisition and Methodology

The aeromagnetic data for the study area were taken from aerial magnetic and gamma-ray spectral surveys, carried out by Aero-Service Division of Western Geophysical Company of America. The airborne geophysical survey was planned to be as a series of parallel flight traverse lines, in the NE–SW direction with 1.5 km spacing. The tie lines were perpendicular to the flight traverse lines (NW–SE direction) and spaced about 10 km. Aeromagnetic measurements were collected using a Varian (V-85) proton free-precession magnetometer sensor, with a sensitivity of 0.1 nT. The nominal flight altitude was 120 meters above the ground surface (Aero-Service, 1984). To make the raw magnetic data appropriate for analysis and interpretation, certain corrections were made, such as error removals associated with acquisition system, diurnal variations, parallax/lag correction, and heading correction. Besides, removal of International Geomagnetic Reference Field (IGRF). Aero-Service (1984) made all these corrections.

3.1 Reduction to The Magnetic Pole

Reduction to the pole (RTP) is a mathematical approach, that transfers the total magnetic data anywhere into magnetic anomaly as if measured at the magnetic pole. It was proposed by to eliminate unwanted distortion in the shapes, sizes, and locations of the magnetic anomalies, due to the influence of inclination and declination of the Earth's magnetic field (Baranov, 1957; Baranov and Naudy, 1964). Therefore, the transform of RTP provides a more precise estimation of the position of magnetic sources, and the shape is easier to interpret from the perspective of the body. This process was done (Aero-Service, 1984).

3.2 Edge Enhancement Techniques

Vertical and horizontal derivatives of the potential field data are used to enhance the edges of anomalies and significantly improve the visibility of these features. Many techniques were developed to delineate structural geological features from potential field data**.** Oasis Montaj 8.4 (Geosoft™) software was used to process and enhance the RTP aeromagnetic data. Evjen was the first to use the first-order vertical derivative (FVD) to define the boundaries of gravity and magnetic bodies (Evjen, 1936). FVD is typically applied to identify the near-surface (shallower) geological structures, where zero values of the FVD of the RTP magnetic field typically refers to geologic body edges (Oruc and Keskinsezer, 2008). It is given as follows:

$$FVD = \frac{\partial M}{\partial z} \quad (1)$$

where, $\frac{\partial M}{\partial z}$ is the vertical derivative of the magnetic anomaly field (M).

It is commonplace to map the edges of magnetic susceptibility contrasts using the horizontal gradient magnitude (HGM) approach. It makes use of the fact that, when the edges of the anomalous body are vertical and widely spaced from one another, the HGM of the RTP magnetic field produced by a tabular body tends to have maximum values there (Cordell and Grauch, 1985). HGM is robust in detecting shallow magnetic sources, and is less sensitive to noise in the data (Philips, 2002). It has amplitude maxima over the magnetic source edges. According to HGM is formulated as follows (Cordell and Grauch, 1985):

$$HGM = \sqrt{\left(\frac{\partial M}{\partial x}\right)^2 + \left(\frac{\partial M}{\partial y}\right)^2} \quad (2)$$

where, $\frac{\partial M}{\partial x}$ and $\frac{\partial M}{\partial y}$ are the horizontal derivatives of the magnetic anomaly field (M) in x and y directions, respectively.

In addition, the analytic signal (AS) method represents also one of the main edge enhancement methods. It reduces the total magnetic field data to anomalies whose maxima define the magnetized body edges, when the sources are resolvable (Nabighian, 1984; Roest et al., 1992; MacLeod et al., 1993). However, they appear as a cluster of highs for a group of near-by sources, regardless of the regional direction of the magnetic field and the magnetization of the source. The equation of AS is as follows:

$$|AS(x,y)| = \sqrt{\left(\frac{\partial M}{\partial x}\right)^2 + \left(\frac{\partial M}{\partial y}\right)^2 + \left(\frac{\partial M}{\partial z}\right)^2} \quad (3)$$

where, $|AS(x,y)|$ is the amplitude of analytic signal at (x,y), $\frac{\partial M}{\partial x}$, $\frac{\partial M}{\partial y}$ and $\frac{\partial M}{\partial z}$ are the derivatives of the magnetic anomaly field (M) in x, y and z directions, respectively.

Predominatingly, the magnetic anomalies due to deep sources are covered by shallow ones, therefore, the tilt angle (TDR) was first proposed by Miller and Singh (1994) for identifying the boundaries of magnetic sources at different depths. It is less affected by the depth of buried magnetic sources and can simultaneously enhance the boundaries of sources of different anomalous amplitudes. Nevertheless, the localized boundaries positions are strongly influenced by the direction of magnetization. TDR is given as follows:

$$TDR = \theta = tan^{-1}\left(\frac{FVD}{HGM}\right) \quad (4)$$

where, FVD and HGM are the vertical derivative and total horizontal derivative of the potential field, respectively.

Several improved methods were developed, based on the aforementioned methods, such as the following:

Theta (Cos θ) method uses the analytic signal (AS) amplitude to normalize the total horizontal derivative (HGM) in a 2D-image (Wijns et al., 2005). It is calculated as follows:

$$Theta = cos(\theta) = \left(\frac{HGM}{AS}\right) \quad (5)$$

Due to the fact that response from deeper sources is more diffuse, the amplitude of responses from different depths are similar on the theta map (Cooper and Cowan, 2006). Edges can be detected with this technique, independent of strike and amplitude.

Cooper and Cowan describe the horizontal tilt angle (TDX) method as the normalization of the HGM by the absolute value of the FVD (Cooper and Cowan, 2006). It is given as follows:

$$TDX = tan^{-1}\left(\frac{HGM}{|FVD|}\right) \quad (6)$$

TDR is effective when dealing with data from shallow sources, while it is regarded relatively inefficient when dealing with data from deep sources. TDX is the inverse of the intended TDR, as it works equally well with shallow and deep sources. One downside of this method is that it reflects edges larger than the actual body size, if there is more than one causative body with different geometries (Cooper and Cowan, 2006).

3.3 Basement Depth Estimation

To determine the depth to the magnetic basement, the source parameter imaging (SPI) technique was used to the RTP aeromagnetic anomaly grid, as this technique is based on the relationship between source depth and the local wave number (K) of the observed field's analytic signal (Thurston and Smith, 1997). It is not affected by remanent magnetization or other magnetic factors such as inclination, declination, dip, and strike.

$$\text{Depth} = 1/K_{max} \quad (7)$$

where, K_{max} is the peak value of the local wavenumber over the step source.

4. Results and Discussion

The colour-shaded grid of RTP magnetic map (Figure 4) is distinguished by the presence of low-and high-amplitude magnetic anomalies scattered throughout the area of study. Generally, the deformation and heterogeneity in the basement rocks produce magnetic signatures, that are both sharp and strong. A detailed comparison of the RTP aeromagnetic map (Figure 4) and the geologic map of the area (Figure 2) shows that, areas of high magnetic anomalies (high-amplitude anomalies), are related to different lithologic units, such as mafic volcanic rocks and serpentinite rocks at the southwestern, northwestern and southern parts, as well as gabbroic rocks in northern and southern parts of the study area. Notably, these anomalies have elongated shapes, which indicate various structural processes that occurred in the study area and their major trend is in the NW–SE direction.

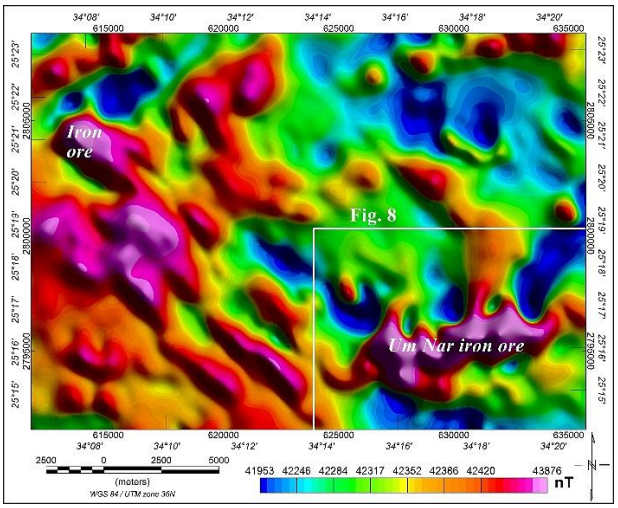

Figure 4: Reduced to the pole (RTP) aeromagnetic map of Wadi Um Nar area, Central Eastern Desert, Egypt (Aero-Service, 1984).

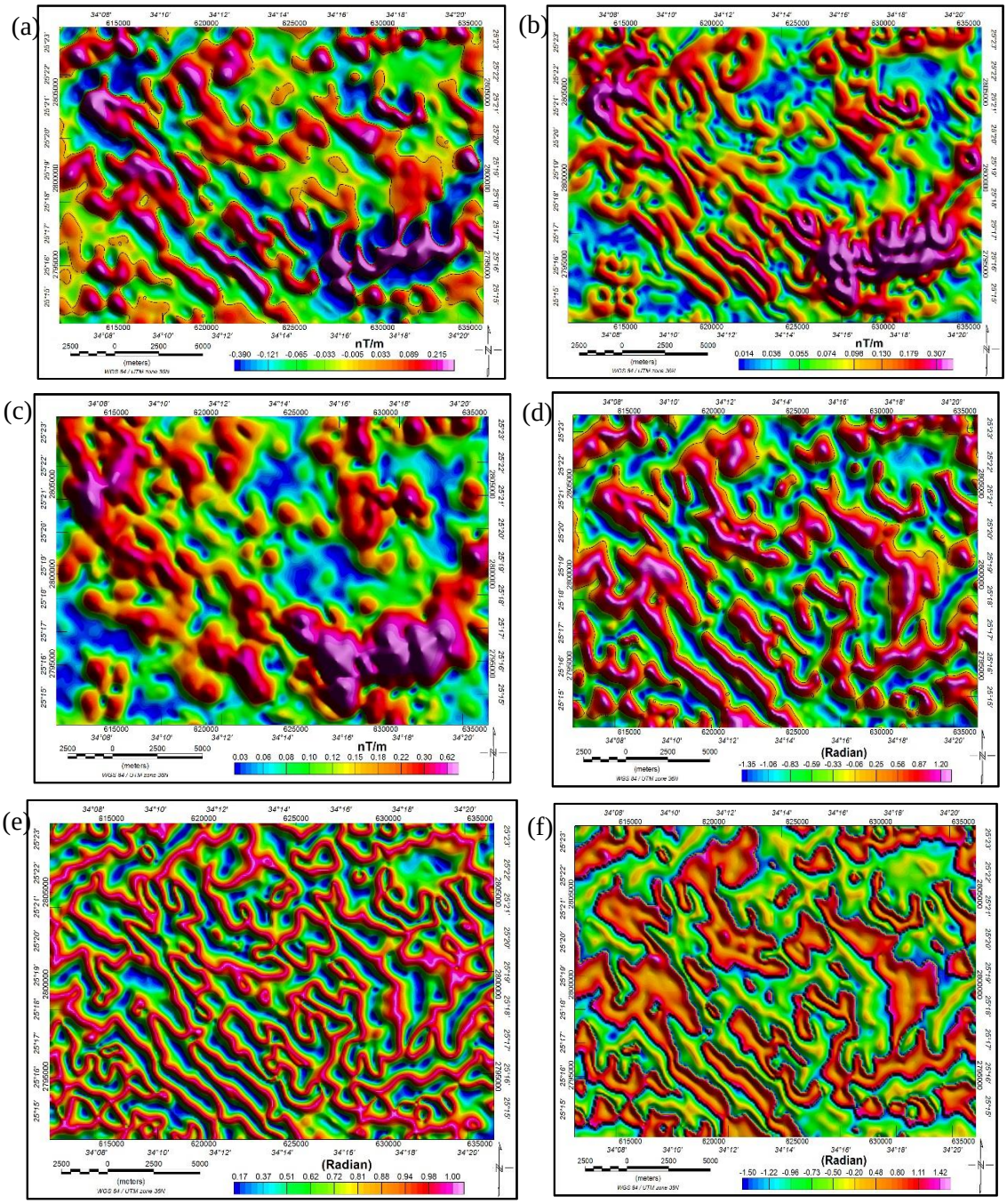

Figure 5: Application of edge enhancement techniques to aeromagnetic data. (a) FVD, (b) HGM, (c) AS, (d) TDR, (e) Theta map and (f) TDX maps of Wadi Um Nar area, Central Eastern Desert, Egypt.

Both Wadi Um Nar and G. El-Hadid BIFs are also located within areas of high positive magnetic anomalies, with peak intensities of over 43,800 nT. Besides, Wadi Um Nar BIFs magnetic anomalies have an E–W trend, while, a NW–SE trend is associated with the magnetic anomalies of G. El-Hadid BIFs. Moreover, a third trend is represented in the NE–SW direction that is accompanied by low magnetic intensity response (low-amplitude anomalies) in the eastern and northwestern parts. These dominant trends suggest that, the study area was subjected to more than single tectonic event. Both the geological map (Figure 2) and the RTP aeromagnetic map (Figure 4) demonstrate substantial connections between the exposed geologic units and the strong magnetic signatures, which may indicate that the magnetic anomalies correlate to the boundaries of geologic structures.

Derivative methods are considered rapid means of processing grids of magnetic data. They supply precise information on the structural framework, tectonic tendencies, and depths. Nevertheless, the structural setting in Wadi Um Nar area is complicated, that it requires an integrated approach that uses different methods. The results from applying the edge enhancement techniques including FVD, HGM, AS, TDR, Theta (Cos θ) and TDX on the RTP magnetic data were shown on Figure 5. According to different algorithms, FVD (Figure 5a) and TDR (Figure 5d) use their zero contour lines (black lines in the figures) as the edges of the magnetic anomaly (faults/boundaries of the magnetic sources). Meanwhile, HGM (Figure 5b), AS (Figure 5c), Theta map (Figure 5e) and TDX (Figure 5f) are represented by their maxima values (peaks).

The resulting maps (Figure 5) show that these edge enhancement techniques are extremely suitable for mapping structures of the basement. Many of the detailed anomalies can be noticed and distinguished by these derivatives of weakly and strongly magnetized source bodies with comparable solutions. These anomalies do not appear clearly on the RTP (Figure 4) magnetic map, especially in the northeastern and southwestern parts of the study area. FVD, HGM and TDR maps (Figures 5a, b and d) illustrate that the southern to the northwestern parts of the study area are dissected by several shallow faults (FVD map), which can extend deep into the basement (HGM and TDR maps). AS map (Figure 5c) highlights the presence of high susceptibility iron-bearing units and show clearly the main east–west trending ore zone, which is related to Wadi Um Nar BIF. Besides, obvious northwest–southeast trend that extends from Wadi Um Nar to G. El-Hadid BIF, is noticed in the northwestern part of the area under study. There is a great similarity between FVD, HGM, TDR, Theta and TDX maps (Figures 5a, b, d, e and f). In comparison with other derivative techniques, Theta and TDX provide more detailed and clear results for more deep magnetized structures as well as a clear and acute response on boundaries of magnetic sources.

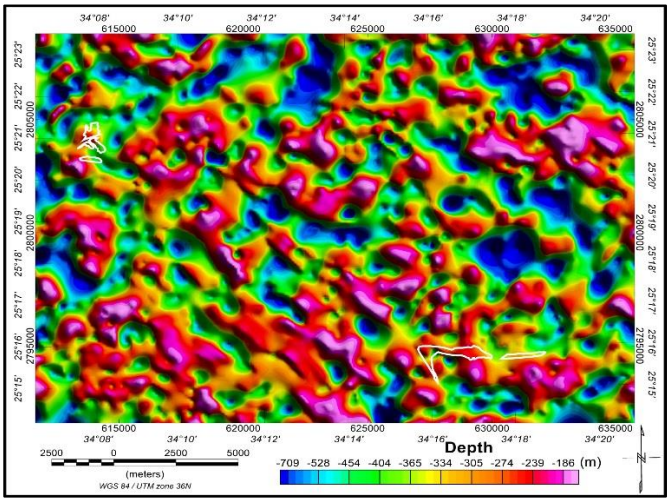

Figure 6: Calculated-depth map to magnetic sources, using source parameter imaging (SPI) of Wadi Um Nar area, Central Eastern Desert, Egypt. White lines are the banded iron formations (BIFs) boundaries.

Figure 6 illustrates variation on depth of different magnetic sources inside the area of study. The demonstrated depths estimated from the sensor height of 120 m above ground level. The majority of target anomalies, specified as resulting from BIF mineralization, occur in areas that have depths less than 450 m from the ground surface. Areas of prospecting are inferred by delineating the boundaries of intrusive rocks via edge enhancement techniques. The structural characteristics that control the accumulation of iron ores in the study area are refined in a detailed structural map, generated by the integration of the obtained results (Figure 7a). When creating a structural map, only the structural elements (faults and contacts) confirmed by various methods were selected. It can be noticed that there is a significant shear zone that extends from the southern part towards the northwestern part of the study area, and trends in a NW–SE direction. Besides, another shear zone is located in the southeastern corner of the study area and trends in an E–W direction (these shear zones are shown in Figure 7a with a grey background colour). Each structural lineament (Figure 7a) reflects multiple intersection zones across this direction. The rose diagram (Figure 7b) shows that, the major dominant tectonic tendencies in the area are NW–SE (Suez Gulf trend), NE–SW (Gulf of Aqaba trend) and N–S trend.

(a)

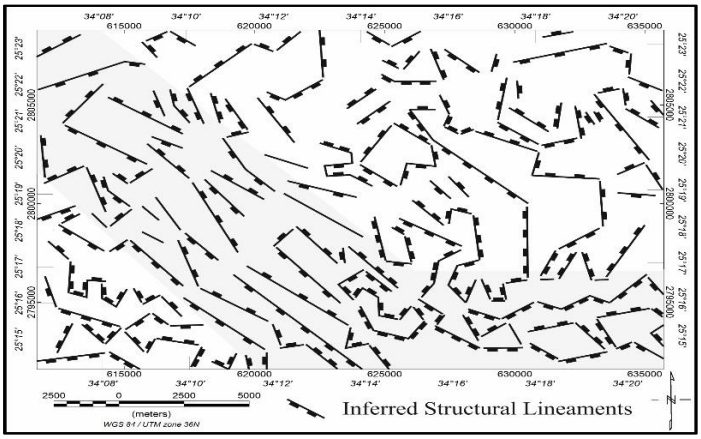

(b)

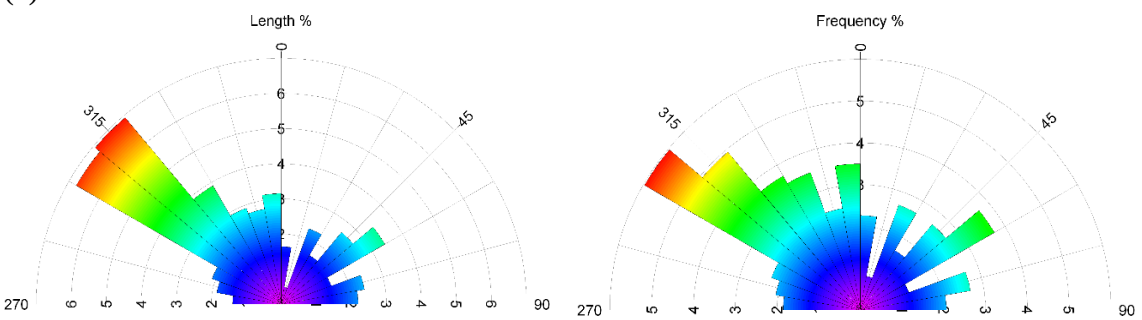

Figure 7: (a) Interpreted structural lineaments map and (b) Directional analysis (rose diagram) of lineament lengths (%) and lineament frequencies (%) of Wadi Um Nar area, Central Eastern Desert, Egypt.

4.1 The Um Nar Iron Ore Deposits

Oasis Montaj 8.4 (Geosoft™) software was used to window a subset grid (from a rectangular mask) in the large RTP map (Figure 4). The subset grid is shown on Figure 8 and represents the anomaly of Um Nar iron ore. The horizontal magnetic field derivatives, in the X (East) and Y (North) directions, are very useful in resolving composite and complex anomalies into their individual components (Aziz et al., 2013). The vertical magnetic field derivative, in the Z (Down) direction, can enhance and highlight the shallow buried features, at the expense of the regional magnetic gradient. Oasis Montaj software was used to perform the orthogonal derivative calculations, and the results were plotted on the maps (Figures 8b–d).

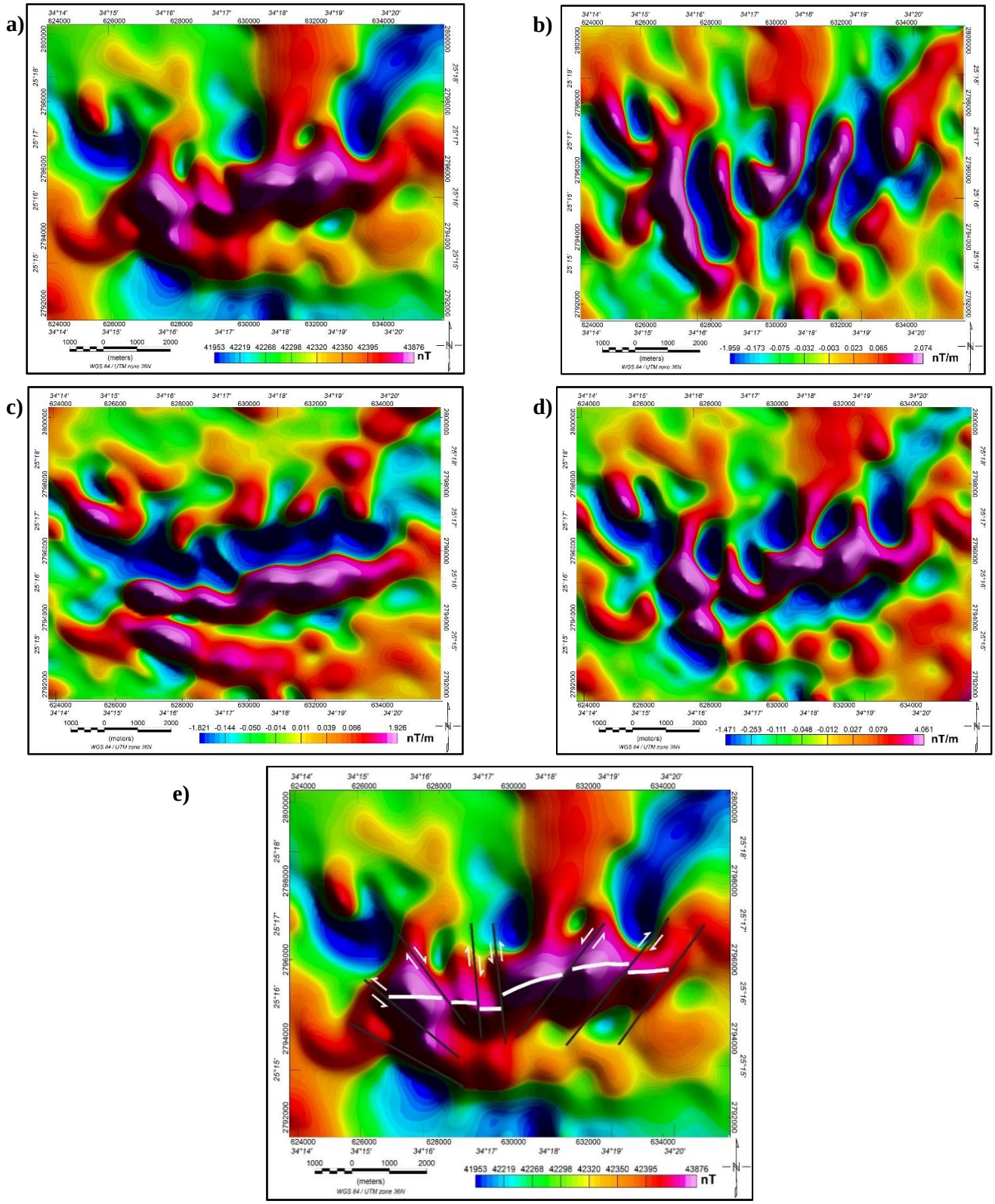

Figure 8: (a) Reduced to the pole (RTP) magnetic map and their orthogonal derivatives in the X (East) direction (b), in the Y (North) direction (c), Vertical derivative in the Z (Down) direction (d) and RTP map with interpreted magnetic structural lineament patterns (e) of Um Nar iron ore, Central Eastern Desert, Egypt.

The Y-derivative map (Figure 8c) shows that, the main east-west ore body has a distinguished dipole response with an inflection point, which roughly corresponds to the maximum amplitude in the RTP map (Figure 8a). The X-derivative map (Figure 8b) identifies also the anomalies of BIFs as dipoles, consisting of multiple dipolar targets. From the horizontal derivatives (X and Y) of the RTP aeromagnetic maps (Figures 8b, c), it can be seen that the structural trends in both x and y directions are improved and clearly visible compared to other aeromagnetic maps. The vertical magnetic field derivative map (Figure 8d) shows a similar general anomaly pattern to the RTP grid map (Figure 8a) but with enhanced

magnetic lineaments, which define the structures affecting the main ore body zone. These interpreted structural lineaments clearly cut the east–west ore body with a lateral displacement and, therefore, can be interpreted as fault or shear zones. This map (Figure 8d) also shows that, the magnetic anomaly over the BIF is dominated by a positive anomaly surrounded by negative anomalies, which may indicate the possibility that the BIFs were remagnetized, since the time of impact. The NW–SE, NE–SW and N–S striking interpreted structural lineaments (Figure 8e) cutting the iron ore zone may be interpreted as brittle faults or shear zones and are probably acted as channels for hydrothermal fluids movement along these fault zones, resulting in the transition of magnetite to other minerals, and consequently leading to local decreases in the magnetic susceptibility of rocks.

The integration of the magnetic data available with the existing geological map (Figure 2) proved to be useful for the litho-structural mapping of the Um Nar iron-ore area (Figure 9), where it is classified into three distinctive lithologic units. These lithological units are: (1) Weakly-magnetic lithology (e.g., granitized terrains; carbonate to low- grade metasediments; felsic- and meta-intrusives; and/or down-faulted blocks); (2) Moderately-magnetic lithology (e.g., intermediate intrusives or meta-intrusives; high-grade metasediments); and (3) Highly-magnetic lithology (e.g., mafic intrusives or meta-intrusives; sedimentary iron formations). Besides, the highly-magnetic lithological unit was intruded by supra-basement or intrasedimentary magnetic bodies (e.g., basic dikes and veins). These magnetic bodies are enriched by the presence of BIFs (as Um Nar zone). They were formed by intruding magma along the structural lineaments and fractures, with the intrusions which are characterized by shallow depths (Figure 6). They were dissected by strike-slip faults, trending in NE–SW, NW–SE and N–S directions.

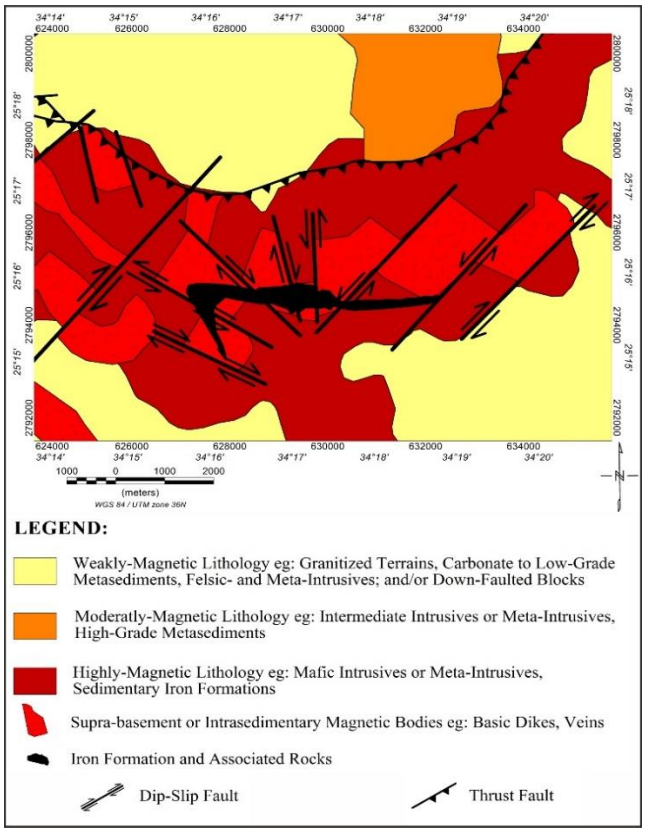

Figure 9: Lithology and structural elements interpreted from magnetic data of Um Nar iron ore zone, Central Eastern Desert, Egypt.

5. Conclusions

The aeromagnetic survey data for Wadi Um Nar area was processed using a set of edge enhancement techniques. The distributions of the BIFs in the study area are mainly associated with high-response magnetic zones and, hence, magnetic structures. The results of edge enhancement techniques helped to identify the inferred magnetic structural lineament map that affected the study area. It was found that the geologic features generally agree with prominent NW–SE, NE–SW and N–S structural trends. Diverse trends of geological features and structural patterns indicate that the study area has experienced more than one tectonic event. The basement depth estimation using SPI shows that the depth to the BIFs varied from the surface up to about 450 m deep. The east–west belt of Wadi Um Nar iron ore corresponds exactly to the zone of highest magnetic intensity. The pattern of complex dipole anomalies within this zone indicates that the iron ore deposits are not simple tabular bodies, but characterized by podiform magnetite deposits, with a general strike of east-west direction. The structural trends of the NW–SE, NE–SW and N–S pattern, defined by magnetic features within the iron ore zone, indicates the presence of faulting or shearing of Wadi Um Nar zone and suggests a complex and multistage deformational history. This study shows that, the BIFs of the study area were produced by magnetite formed in structurally controlled fluid flow regions.

Acknowledgment

The author extends sincere thanks to Prof. Dr. Ahmed A. Ammar and Prof. Dr. Alaa Aref, Exploration Sector, Nuclear Materials Authority of Egypt, for their critical and constructive review of the manuscript, and for their fruitful discussions.

References

Abdelrahman, E.M., Essa, K.S., 2015. A new method for depth and shape determinations from magnetic data. Pure and Applied Geophysics, 172, Pp. 439–460.

Abo-Ezz, E.R., Essa, K.S., 2016. A least-squares minimization approach for model parameters estimated by using a new magnetic anomaly formula. Pure Appl Geophys., 173, Pp. 1265–1278.

Abu El Ela, A.M., 1985. Geology of Wadi Mubarak District, Eastern Desert, Egypt. Ph.D. Thesis, Tanta University, Tanta, Egypt, Pp. 359.

Aero-Service, 1984. Final Report on airborne magnetic and radiation survey in Eastern Desert, Egypt. Work Completed for the Egyptian General Petroleum Corporation (EGPC), Six Volumes, Aero-Service, Houston, Texas, USA.

Akaad, M.K., Noweir, A.M., Abu El Ela, A.M., 1995. The Volcanosedimentary association and ophiolites of Wadi Mubarak, Eastern Desert, Egypt. In: Proc. Int. Conf. 30 years Cooper. Geological Survey, Egypt, Spec. Publ. 69, Pp. 231–248.

Akaad, M.K., Noweir, A.M., Abu El Ela, A.M., 1996. Geology of the Pan-African Basement Rocks of the Jabal El Hadid–Wadi Mubarak district, E.D., Egypt, Covering Parts of Sheets NG 36 G 3, 6 and NG 36 H 1, 4. Geological Survey, Egypt, No. 73, Pp. 78.

Ali, K.A., Stern, R.J., Manton, W.I., Kimura J.I., Khamees, H.A., 2009. Geochemistry, Nd isotopes and U-Pb SHRIMP zircon dating of Neoproterozoic volcanic rocks from the Central Eastern Desert of Egypt: New insights into the ~750 Ma crust-forming event. Precambr. Res. 171, Pp. 1–22.

Aziz, A.M., Sauck, W.A., Shendi, E.H., Rashed, M.A., Abd El-Maksoud, M., 2013. Application of Analytic Signal and Euler Deconvolution in Archaeo-Magnetic Prospection for Buried Ruins at the Ancient City of Pelusium, NW Sinai, Egypt: A Case Study. Surv Geophys., 34, Pp. 395–411. DOI 10.1007/s10712-013-9229-z

Baranov, V., 1957. A new method for interpretation of aeromagnetic maps pseudo gravimetric anomalies. *Geophysics*, 22, Pp. 359–383.

Baranov, V., Naudy, H., 1964. Numerical calculation of the formula of reduction to the magnetic pole. Geophysics, 29, Pp. 67–79.

Basta, F.F., Maurice, A.E., Fontbote, L., Favarger, P.Y., 2011. Petrology and geochemistry of the banded iron formation (BIF) of Wadi Karim and Um Anab, Eastern Desert, Egypt: implications for the origin of Neoproterozoic BIF. Precambr. Res., 187 (3–4), Pp. 277–292.

Bekker, A., Slack, J.F., Planavsky, N., Krapez, B., Hofmann, A., Konhauser, K.O., Rouxel, O.J., 2010. Iron formation: the sedimentary product of a complex interplay amongmantle, tectonic, oceanic, and biospheric processes. Economic Geology, 105, Pp. 467–508.

Boufkri, H., El Azzab, D., Miftah, A., 2023. Airborne data processing and 3D modeling of magnetic structures between Nador region and the Chaffarine Islands: Geological significances. Journal of King Saud University – Science, 35, Pp. 102380. https://doi.org/10.1016/j.jksus.2022.102380

Cooper, G.R.J., Cowan, D.R., 2006. Enhancing potential field data using filters based on the local phase. Comput. Geosci., 32, Pp. 1585–1591.

Cordell, L., Grauch, V.J.S., 1985. Mapping basement magnetization zones from aeromagnetic data in the San Juan basin, New Mexico. In The Utility of Regional Gravity and Magnetic Anomaly Maps; Hinzc, W.J., Ed.; Society of Exploration Geophysicists: Tulsa, OK, USA, Pp. 181–197.

Dardir, A.A., El Shimi, A.M., 1992. Geology and geochemical exploration for gold in the banded iron formation of Um Nar area, Central Eastern Desert, Egypt. Ann Geol Survey Egypt XVIII: Pp. 103–111.

Ekwok, S.E., Eldosouky, A.M., Ben, U.C., Alzahrani, H., Abdelrahman, K., Achadu, O.I.M., Pham, L.T., Akpan, A.E., Gómez-Ortiz, D., 2022. Application of High-Precision Filters on Airborne Magnetic Data: A Case Study of the Ogoja Region, Southeast Nigeria. Minerals, 12, Pp. 1227. https://doi.org/10.3390/min12101227

El Aref, M.M., Abdel Wahed, M., El Dougdoug, A., Manawi, A., 1993a. Geological setting and deformational history of Umm Nar BIF and associated rocks, Eastern Desert, Egypt. Egyptian Journal of Geology, 37, Pp. 205–230.

El Aref, M.M., Abdel Wahed, M., El Dougdoug, A., Manawi, A., 1993b. Diagenetic and metamorphic history of the Umm Nar BIF, Eastern Desert, Egypt. Mineralium Deposita 28, Pp. 264–278.

El Bahariya, G.A., 2018. Classification of the Neoproterozoic ophiolites of the Central Eastern Desert, Egypt based on field geological characteristics and mode of occurrence. Arab J Geosci., 11, Pp. 313. https://doi.org/10.1007/s12517-018-3677-1

El Bahariya, G.A., 2021. The Ophiolite-Dominated Suprastructure, Eastern Desert, Egypt. In: Hamimi, Z., Arai, S., Fowler, AR., El-Bialy, M.Z. (eds) The Geology of the Egyptian Nubian Shield. Regional Geology Reviews. Springer, Cham. https://doi.org/10.1007/978-3-030-49771-2_6

El Habaak, G.H., 2004. Pan-African skarn deposits related to banded iron formation, Um Nar area, central Eastern Desert, Egypt. J. Afr. Earth Sci., 38 (2), Pp. 199–221.

El Habaak, G.H., 2021. Banded Iron Formation in the Egyptian Nubian Shield. In: Hamimi, Z., Arai, S., Fowler, AR., El-Bialy, M.Z. (eds) The Geology of the Egyptian Nubian Shield. Regional Geology Reviews. Cham, Switzerland: Springer Nature Switzerland AG, Pp. 425-486. https://doi.org/10.1007/978-3-030-49771-2_17

El Habaak, G.H., Mahmoud, M.S., 1994. Carbonaceous bodies of debatable organic provenance in the Banded Iron Formation of Wadi Kareim area, Eastern Desert, Egypt. J Afr Earth Sci., 19, Pp. 125–133.

Elhussein, M., Shokry, M., 2020. Use of the airborne magnetic data for edge basalt detection in Qaret Had El Bahr area, Northeastern Bahariya Oasis, Egypt. Bulletin of Engineering Geology and the Environment. https://doi.org/10.1007/s10064-020-01831-w.

Elhusseiny, A.A., 2023. Integrated Structure and Mineralization Study Using Aero-Magnetic, Aero-Spectrometric and Remote Sensing Data at Esh El-Mallaha Area, Eastern Desert, Egypt. Geomaterials, 13, Pp. 1-22. https://doi.org/10.4236/gm.2023.131001

El-Ramly, M.F., Akaad, M.K., Rasmy, A.H., 1963. Geology and structure of Umm Nar iron ore deposit (Eastern Desert of Egypt). Geological Survey and Mineral Research Department Paper No. 28 Egyptian Geological Survey, Cairo, Egypt. (United Arab Republic (Egypt), Pp. 30.

El-Shazly, A.K., Khalil, K.I., 2014. Banded iron formations of Um Nar, Eastern Desert of Egypt: P–T–X conditions of metamorphism and tectonic implications. Lithos, Volumes 196–197, Pp. 356–375. https://doi.org/10.1016/j.lithos.2014.01.006

El-Shazly, A.K., Khalil, K.I., Helba, H.A., 2019. Geochemistry of banded iron formations and their host rocks from the Central Eastern Desert of Egypt: A working genetic model and tectonic implications. Precambrian Research, 325, Pp. 192–216. https://doi.org/10.1016/j.precamres.2019.02.011.

Essa, K.S., Diab, Z.E., 2022. Magnetic data interpretation for 2D dikes by the metaheuristic bat algorithm: sustainable development cases. Scientific Reports, 12, Pp. 14206. https://doi.org/10.1038/s41598-022-18334-1

Essa, K.S., Elhussein, M., 2017. A new approach for the interpretation of magnetic data by a 2-D dipping dike. J. Appl. Geophys., 136, Pp. 431–443.

Evjen, H.M., 1936. The place of the vertical gradient in gravitational interpretations. Geophysics, 1, Pp. 127–136.

Eyles, N., Januszczak, N., 2004. 'Zipper-rift': a tectonic model for Neoproterozoic glaciations during the breakup of Rodinia after 750 Ma. Earth Sci. Rev., 65 (1), Pp. 1–73.

Farhi, W., Boudella, A., Saibi, H., Bounif, M.O.A., 2016. Integration of magnetic, gravity, and well data in imaging subsurface geology in the Ksar Hirane region, Laghouat, Algeria. J. Afr. Earth Sci., 124, Pp. 63–74.

Freitas, B.T., Warren, L.V., Boggiani, P.C., De Almeida, R.P., Piacentini, T., 2011. Tectono-sedimentary evolution of the Neoproterozoic BIF-bearing Jacadigo Group, SW-Brazil. Sediment. Geol., 238 (1), Pp. 48–70.

Gross, G.A., 1996. Algoma-type Iron-formation. In: Lefebure, D.V., Hoy, T. (Eds.), Selected British Columbia Mineral Deposit Profiles, Volume 2 — Metallic Deposits. British Columbia Ministry of Employment and Investment, Open File 1996-13, Pp. 25–28.

Henderson, I.H.C., Viola, G., Nasuti, A., 2015. A new tectonic model for the Kautokeino Greenstone Belt, northern Norway, based on high-resolution airborne magnetic data and field structural analysis and implications for mineral potential. Norwegian Journal of Geology, 95, Pp. 339–363. http://dx.doi.org/10.17850/njg95-3-05.

Holden, E.J., Wong, J.C., Kovesi, P., Wedge, D., Dentith, M., Bagas, L., 2012. Identifying structural complexity in aeromagnetic data: An image analysis approach to greenfields gold exploration. Ore Geology Reviews, 46, Pp. 47-59. https://doi.org/10.1016/j.oregeorev.2011.11.002

Isley, A.E., 1995. Hydrothermal plumes and the delivery of iron to banded iron formation. J. Geol., 103 (2), Pp. 169–185.

Isley, A.E., Abbott, D.H., 1999. Plume-related mafic volcanism and the deposition of banded iron-formation. J. Geophys. Res., 104, Pp. 15461–15477.

Kassem, O.M.K., 2011. Determining heterogeneous deformation for granitic rocks in the northern thrust in Wadi Mubarak belt, Eastern Desert, Egypt. Geotectonics, 45, Pp. 244–254. https://doi.org/10.1134/S0016852111030046

Kassem, O.M.K., 2012. Kinematic vorticity technique for porphyroclasts in the metamorphic rocks: an example from the northern thrust in Wadi Mubarak belt, Eastern Desert, Egypt. Arab J Geosci., 5, Pp. 159–167. https://doi.org/10.1007/s12517-010-0229-8

Khalil, K.I., El-Shazly, A.E., Lehmann, B., 2015. Late Neoproterozoic banded iron formation (BIF) in the Central Eastern Desert of Egypt: Mineralogical and geochemical implications for the origin of the Gebel El Hadid iron ore deposit. Ore Geol. Rev., 69, Pp. 380–399. http://dx.doi.org/10.1016/j.oregeorev.2015.02.017.

Klein, C., 2005. Some Precambrian banded iron formations from around the world: their age, geologic setting, mineralogy, metamorphism, geochemistry, and origin. American Mineralogist, 90, Pp. 1473–1499.

Klein, C., Beukes, N.J., 1993. Proterozoic Iron-formations. In: Condie, K.C. (Ed.), Development in Precambrian Geology: Proterozoic crustal, evolution, 10, Pp. 383–418.

Loizenbauer, J., Wallbrecher, E., Fritz, H., Neumayr, P., Khudeir, A., Kloetzli, U., 2001. Structural Geology, single zircon ages and fluid inclusion studies of the Meatiq metamorphic core complex: Implications for Neoproterozoic tectonics in the Eastern Desert of Egypt. Precambr. Res., 110 (1), Pp. 357–383.

MacLeod, I.N., Jones, K., Dai, T.F., 1993. 3-D analytic signal in the interpretation of total magnetic field data at low magnetic latitudes. Exploration Geophysics, 24, Pp. 679-688.

Makroum, F., 2003. Lattice preferred orientation (LPO) study of the orogeny parallel Wadi Nugrus and Wadi Um Nar shears, Eastern Desert, Egypt, using EBSD technique. In: Proceedings of the second international conference on the geology of Africa: Egypt: Assiut, Egypt, Assiut University, 1, Pp. 213–232.

Miller, H.G., Singh, V., 1994. Potential Field Tilt—A New Concept for Location of Potential Field Sources. J. Appl. Geophys., 32, Pp. 213–217.

Mücke, A., Annor, A., Neumann, U., 1996. The Algoma-type iron-formations of the Nigerian metavolcano-sedimentary schist belts. Mineral. Deposita, 31, Pp. 113–122.

Nabighian, M.N., 1984. Toward a three-dimensional automatic interpretation of potential field data via generalized Hilbert transforms: fundamental relations. Geophysics, 49 (6), Pp. 780-786.

Nabighian, M.N., Grauch, V.J.S., Hansen, R.O., LaFehr, T.R., Li, Y., Peirce, J.W., Ruder, M.E., 2005. The historical development of the magnetic method in exploration. Geophysics, 70 (6), Pp. 33ND-61ND.

Nadoll, P., Angerer, T., Mauk, J.L., French, D., Walshe, J., 2014. The chemistry of hydrothermal magnetite: A review. Ore Geology Reviews, 61, Pp. 1–32. https://doi.org/10.1016/j.oregeorev.2013.12.013

Neumayr, P., Hoinkes, G., Puhl, J., Mogessie, A., Khudeir, A., 1998. The Meatiq dome (Eastern Desert, Egypt) a Precambrian metamorphic core complex: petrological and geological evidence. Journal of Metamorphic Geology, 16 (2), Pp. 259–279.

Ohmoto, H., Watanabe, Y., Yamaguchi, K.E., Naraoka, H., Haruna, M., Kakegawa, T., Hayashi, K.I., Kato, Y., 2006. Chemical and biological evolution of early Earth: constraints from banded iron formations. Geol. Soc. Am. Mem., 198, Pp. 291–331.

Oruç, B., Keskinsezer, A., 2008. Structural setting of the northeastern Biga Peninsula (Turkey) from tilt derivatives of gravity gradient tensors and magnitude of horizontal gravity components. Pure Appl. Geophys., 165, Pp. 1913–1927.

Phillips, J.D., 2002. Processing and Interpretation of Aeromagnetic Data for the Santa Cruz Basin-Patahonia Mountains Area, South-Central Arizona; U.S. Geological Survey Open-File Report 02-98; U.S. Geological Survey: Reston, VA, USA.

Rasmy, A.H., 1968. Mineralogical and lithological studies of the Umm Nar iron ore deposit, Eastern Desert, Egypt. M.Sc. thesis, Assiut University, Egypt, Pp. 121, unpublished.

Roest, W.R., Verhoef, J., Pilkington, M., 1992. Magnetic interpretation using the 3-D analytic signal. Geophysics, 57, Pp. 116-125.

Shah, A.K., Bedrosian, P.A., Anderson, E.D., Kelley, K.D., Lang, J., 2013. Integrated geophysical imaging of a concealed mineral deposit: A case study of the world-class Pebble porphyry deposit in southwestern Alaska: Geophysics, 78 (5), Pp. B317–B328. doi: 10.1190/geo2013-0046.1.

Shalaby, A., 2003. Structural and tectonic evolution of the Wadi Mubarak belt, Central Eastern Desert, Egypt. Unpublished Ph.D. Thesis, Graz University, Pp. 178.

Shalaby, A., Stüwe, K., Fritz, H., Makroum, F., 2006. El Mayah molasses basin, Eastern Desert of Egypt. J. Afr. Earth Sci., 45, Pp. 1–15.

Shalaby, A., Stüwe, K., Makroum, F., Fritz, H., Kebede, T., Klötzli, U., 2005. The Wadi Mubarak belt, Eastern Desert of Egypt: a Neoproterozoic conjugate shear system in the Arabian–Nubian Shield. Precambrian Res., 136, Pp. 27–50.

Shebl, A., Abdellatif, M., Elkhateeb, S.O., Csámer, Á., 2021. Multisource Data Analysis for Gold Potentiality Mapping of Atalla Area and Its Environs, Central Eastern Desert, Egypt. Minerals, 11, Pp. 641. https://doi.org/10.3390/min11060641

Silva, A.M., 1999. Integração de dados geológicos e geofísicos utilizando-se uma nova técnica estatística para seleção de alvos para exploração mineral, aplicada ao Greenstone Belt Rio das Velhas, Quadrilátero Ferrífero. Instituto de Geociências, Universidade de Brasília, Brasília, Tese de Doutoramento, Pp. 195.

Sims, M.A., James, H.L., 1984. Banded iron ore formation of Late Proterozoic age in the Central Eastern desert, Egypt: geological and tectonic setting. Economic Geology, 79, Pp. 1777–1784.

Stern, R.J., Mukherjee, S.K., Miller, N.R., Ali, K., Johnson, P.R., 2013. ~750 Ma banded iron formation from the Arabian-Nubian Shield—Implications for understanding Neoproterozoic tectonics, volcanism, and climate change. Precamb Res., 239, Pp. 79–94. https://doi.org/10.1016/j.precamres.2013.07.015.

Telford, W.M., Geldart, L.P., Sheriff, R.E., 1990. Applied geophysics, second edition. Cambridge University Press, Cambridge, Pp. 770.

Thurston, J.B., Smith, R.S., 1997. Automatic conversion of magnetic data to depth, dip, and susceptibility contrast using the SPI (TM) method: Geophysics, 62, Pp. 807–813.

Wijns, C., Perez, C., Kowalczyk, P., 2005. Theta Map: Edge Detection in Magnetic Data. Geophysics, 70, Pp. 39–43.

Zhu, X.Q., Tang, H.S., Sun, X.H., 2014. Genesis of banded iron formations: A series of experimental simulations. Ore Geology Reviews, 63, Pp. 465–469. https://doi.org/10.1016/j.oregeorev.2014.03.009